RSC Advances

PAPER

View Article Online
View Journal | View Issue

Cite this: *RSC Adv.*, 2022, **12**, 28364

Novel imidazolium-thiohydantoin hybrids and their Mn(III) complexes for antimicrobial and anti-liver cancer applications†

Lamia A. Ismail,[a] R. Zakaria,[a] Eman M. Hassan,[a] Mohammad Y. Alfaifi,[b] Ali A. Shati,[b] Serag Eldin I. Elbehairi,[bc] A. A. El-Bindary[d] and Reda F. M. Elshaarawy *[ef]

We present the effective synthesis and structural characterization of three novel imidazolium-thiohydantoin ligands (IMTHs, **5a–c**) and their Mn(III) complexes (Mn(III)IMTHs, **6a–c**) in this study. The findings of elemental analyses, spectral analyses and magnetic measurements will be used to infer the stoichiometry, coordination styles, and geometrical aspects of Mn(III)IMTHs. The new compounds were evaluated for their chemotherapeutic potential against ESKAPE pathogens and liver cancer (HepG2). According to the MIC and MBC values, the bactericidal and bacteriostatic activities of IMTHs have been significantly improved following coordination with the Mn(III) ion. The MTT assay results showed that all Mn(III)IMTHs had the potential to reduce the viability of liver carcinoma (HepG2) cells in a dose-dependent manner, with the BF_4-supported complex (**6b**) outperforming its counterparts (**6a** and **6c**) as well as a clinical anticancer drug (VBL). Additionally, Mn-$IMTH_2$ (**6b**) showed the highest level of selectivity (SI = 32.05) for targeting malignant cells (HepG2) over healthy cells (HL7702).

Received 20th August 2022
Accepted 27th September 2022

DOI: 10.1039/d2ra05233d

rsc.li/rsc-advances

1. Introduction

Treatment of infectious illnesses is still a severe challenge for clinics, despite substantial advances in medicine, because most pathogens are developing multidrug resistance.[1] As estimated by World Health Organization (WHO), 57 million people worldwide die each year from infectious illnesses, and this figure is expected to climb in the coming years due to the extensive distribution of resistance genes in bacteria. In particular, the multidrug-resistant ESKAPE pathogens (*Staphylococcus aureus*, *Pseudomonas aeruginosa*, *Klebsiella pneumoniae*, *Enterococcus faecium*, *Acinetobacter baumannii*, and *Enterobacter* species), pose a great challenge in clinics across the world because they can survive the fatal effects of currently available antimicrobial drugs and induce nosocomial infections.[2] With the decline in the development of novel antimicrobials, antibiotic resistance has risen throughout the world.

The molecular hybridization technique has garnered a lot of attention over the last two decades as a promising strategy for drug discovery and developing novel pharmacophores with biological multifunctions.[3,4] The combination of two separate bioactive compounds with adjuvant properties[5] and differing modes of action might be an appropriate way to boost the potency and increase the selectivity of the hybrid molecule toward pathogens and cancer cells over normal ones and hence reduce their adverse effects.[6,7] However, despite the success of the hybrid method in antimalarial[8] and anticancer[9,10] drug development, there is still a lack of research in the field of antimicrobial agents.

In pharmacological chemistry, the hydantoin/thiohydantoin (TH) ring is well-known as an important pharmacophoric moiety that has been exploited to produce novel potential anticancer drugs such as the androgen receptor antagonist Enzalutamide (ENZ) and its derivatives.[11] Despite its small size, this ring has four functionalization sites and four H-bonding donor/acceptor (HBD/HBA) sites.[11] Therefore, the TH moiety acts as a key pharmacophoric moiety or skeletal component of many hybrid small pharmacological molecules including anticancer,[12–15] antimicrobial,[16,17] anti-inflammatory,[18] anti-leishmanial,[19,20] antidiabetic,[21] antioxidant,[22] anticonvulsant,[23] and anti-HIV.[24] Furthermore, thiohydantoin derivatives are androgen receptor and TNF-antagonists, as well as effective inhibitors of several enzymes, including DNA Topoisomerase I, II (TopI, II), NOXs, isocitrate dehydrogenases (IDHs), B-cell lymphoma-2 (Bcl-2) and sirtuins (SIRTs), kinesin spindle protein (KSP), prolyl

[a]*Department of Chemistry, Faculty of Science, Port Said University, Port Said 42526, Egypt*
[b]*Biology Department, Faculty of Science, King Khalid University, Abha 9004, Saudi Arabia*
[c]*Cell Culture Lab, Egyptian Organization for Biological Products and Vaccines (VACSERA Holding Company), Giza 12311, Egypt*
[d]*Chemistry Department, Faculty of Science, Damietta University, Damietta, 34517, Egypt*
[e]*Department of Chemistry, Faculty of Science, Suez University, Suez 43533, Egypt. E-mail: reda.elshaarawy@suezuniv.edu.eg*
[f]*Institut für Anorganische Chemie und Strukturchemie, Heinrich-Heine Universität Düsseldorf, Düsseldorf, Germany. E-mail: reel-001@hhu.de*

† Electronic supplementary information (ESI) available. See https://doi.org/10.1039/d2ra05233d

hydroxylases 1–3 (PHD 1–3), CDK2, and CDK4.[11,25] It's interesting to note the emergence of the thiohydantoin ring as an efficient pharmacophoric ingredient in the development of potent inhibitors for EGFR and VEGFR growth factor receptors.[26,27] Many hybrid hydantoin/thiohydantoin-supported chemical entities have been approved as clinical medications.[11]

Because of their adjustable features and capacity to fine-tune biological potential, imidazolium ionic liquids (IMILs) have a wide variety of applications.[28,29] Because of their tunable toxicity, IMILs have drawn considerable attention as antimicrobials. So far, investigations on the antimicrobial direct use of IMILs have shown promising outcomes, although they are still in their infancy.[28] Furthermore, IMILs have shown outstanding outcomes even in the situation of biofilm-forming microbes that are resistant to other antimicrobial agents.[30] For instance, the chlorides, bromides, and iodides of 1-alkyl-3-methylimidazolium were active against both planktonic and biofilm-inducing bacteria and fungus.[30] Interestingly, alkyl-3-methylimidazolium fumarates showed excellent antimicrobial activity and were proposed for medicinal application.[31]

As a result of the aforementioned remarkable facts and as part of our ongoing endeavor to create and investigate novel chemotherapeutic candidates,[32–34] the current study aims to design and develop novel imidazolium-thiohydantoin hybrids for antimicrobial, particularly against ESKAPE pathogens, and anticancer applications using a molecular hybridization approach.

2. Experimental

2.1. Materials and methods

2.1.1. Materials. Details about the chemicals (2-*tert*-butylphenol (2-TBP), anhydrous $MgCl_2$ and $Mn(CH_3COO)_2\cdot 4H_2O$, paraformaldehyde, 1-ethylimidazole, triethylamine (Et_3N), LiCl, and anhydrous $ZnCl_2$) and solvents used in this work and their resources were given in the ESI.† Moreover, protocols used for the preparation of the starting materials 3-*tert*-butylsalicylaldehyde (**1**) and 5-chloromethyl-3-*tert*-butylsalicylaldehyde (CMTBS, **2**) were explained in detail in the ESI†.

2.1.2. Instrumentation. The novel compounds were structurally investigated using elemental (CHNS), spectral (FTIR, UV-vis, NMR (^{1}H-NMR, ^{13}C-NMR, ^{11}B-NMR, ^{31}P-NMR, ^{19}F-NMR), and ESI-MS), and magnetic studies. The equipments used to conduct these studies were also discussed in the ESI†.

2.2. Synthesis of 3-(3-(*tert*-butyl)-5-formyl-4-hydroxybenzyl)-1-ethylimidazolium ionic liquids (3a–c)

2.2.1. 3-(3-(*tert*-Butyl)-5-formyl-4-hydroxybenzyl)-1-ethylimidazolium chloride (3a). An anhydrous toluene solution (25 mL) of CMTBS (2) (2.19 g, 10.27 mmol) was added dropwise to a solution of 1-ethylimidazole (1.03 g, 10.71 mmol) in anhydrous toluene (25 mL) under a nitrogen atmosphere while vigorously stirring at room temperature (RT). After that, the content was heated to 60 °C under a nitrogen atmosphere and kept at these conditions while stirring for 24 h. After cooling the reaction mixture, filtration and washing with dry toluene (3 × 5 mL) followed by ether (5 × 10 mL) were used to remove the unreacted materials from the desired solid product (**3a**), which was then dried *in vacuo*. This product was used to prepare the other imidazolium ionic liquids (**3b,c**) without further purification. **3a** was obtained as a white solid, Yield (89%), mp: 73 °C. FTIR (KBr, cm^{-1}): 3429 (m, br, O–H), 3109 (m, sh, aromatic (C–H)$_{asym}$), 3049 (m, sh, aromatic (C–H)$_{sym}$), 2971 (m, sh, aliphatic C–H), 2869 (m, sh, aldehydic C–H), 1645 (*vs.*, sh, C=O), 1541, 1459, 1401 (s, sh), 1271 (s, sh, $\nu_{(Ar-O)}$), 1153 (s, sh, (H–C=C + H–C=N)$_{bend}$ of Imidazolium ring), 745 (m, sh), 671 (m, sh). ^{1}H NMR (200 MHz, $CDCl_3$) δ (ppm): 11.44 (s, 1H, Ar-O**H**), 10.73 (s, 1H, Ar-**H**C=O), 9.91 (s, 1H, Im-**H**), 7.93 (s, 1H, Im-**H**), 7.73–7.34 (m, 2H, Im-**H** and Ar-**H**), 7.34–7.18 (m, 1H, Ar-**H**), 5.61 (s, 2H, N3-C**H$_2$**-Ar), 4.33 (q, J = 7.4 Hz, 2H, N1-C**H$_2$**CH$_3$), 1.55 (t, J = 7.3 Hz, 3H, N1-CH$_2$CH$_3$), 1.34 (s, 9H, C(CH$_3$)$_3$). ^{13}C NMR (125 MHz, $CDCl_3$) δ (ppm): 193.85, 157.55, 141.73, 138.03, 135.96, 131.11, 129.65, 128.37, 123.78, 122.91, 56.21, 42.42, 27.39, 23.63, 15.49. ESI-MS: in positive mode peaks at m/z 287.4 ([$C_{17}H_{23}N_2O_2$, M–Cl$^-$]$^+$) a.m.u.

2.3. Anion exchange; synthesis of (3b,c)

An aqueous solution (25 mL) of **3a** (1.22 g, 3.96 mmol) in deionized water (DIW) was treated with 4.75 mmol (1.2 eq.) of the anion salt (0.52 g of $NaBF_4$ and 0.87 g of KPF_6) while vigorously stirring at RT. After stirring the reaction mixture for 48 h at RT, the isolated solids were collected by filtration and then washed with DIW (to remove any impurities) until obtaining neutral washing liquor. The intended products (tetrafluoroborate (**3b**) and hexafluorophosphate product (**3c**)) were vacuum dried overnight at 40 °C.

2.3.1. 3-(3-(*tert*-butyl)-5-formyl-4-hydroxybenzyl)-1-ethylimidazolium tetrafluoroborate (3b). Yield (83%); mp 89 °C. FT-IR (KBr, cm^{-1}): 3449 (m, br, O–H), 3152 (m, sh, aromatic (C–H)$_{asym}$), 3087 (m, sh, aromatic (C–H)$_{sym}$), 2968 (m, sh, aliphatic C–H) 2874 (m, sh, aldehydic C–H), 1646 (*vs.*, sh, C=O), 1544, 1463, 1392 (s, sh), 1273 (s, sh, Ar–O), 1156 (s, sh, (H–C=C + H–C=N)$_{bend}$ of Imidazolium ring), 1057 (*vs.*, sh, BF_4),749 (s, sh), 675 (m, sh). ^{1}H NMR (200 MHz, DMSO-d_6) δ (ppm): 11.22 (s, 1H, Ar-O**H**), 10.05 (s, 1H, Ar-**H**C=O), 9.28 (s, 1H, Im-**H**), 7.84 (d, J = 1.6 Hz, 1H, Im-**H**), 7.71 (s, 1H, Ar-**H**), 7.35–7.17 (m, 2H, Im-**H** and Ar-**H**), 5.40 (s, 2H, N3-C**H$_2$**-Ar), 4.22 (q, J = 7.2 Hz, 2H, N1-C**H$_2$**CH$_3$), 1.44 (t, J = 7.3 Hz, 3H, N1-CH$_2$CH$_3$), 1.23 (s, 9H, C(CH$_3$)$_3$). ^{13}C NMR (125 MHz, DMSO-d_6) δ (ppm): 193.43, 157.87, 141.89, 137.98, 136.02, 131.07, 129.47, 128.12, 123.78, 122.85, 55.78, 42.16, 27.31, 23.28, 15.34. ESI-MS: in positive mode peaks at m/z 287.4 ([$C_{17}H_{23}N_2O_2$, M–BF_4^-]$^+$) a.m.u.

2.3.2. 3-(3-(*tert*-butyl)-5-formyl-4-hydroxybenzyl)-1-ethylimidazolium hexafluorophosphate (3c). Yield (88%); mp 118 °C. FT-IR (KBr, cm^{-1}): 3439 (m, br, O–H), 3187 (m, sh, aromatic (C–H)$_{asym}$), 3098 (m, sh, aromatic (C–H)$_{sym}$), 2969 (m, sh, aliphatic C–H), 2873 (m, sh, aldehydic C–H), 1646 (*vs.*, sh, C=O), 1543, 1461, 1398 (s, sh), 1270 (s, sh, Ar–O), 1155 (s, sh, (H–C=C + H–C=N)$_{bend}$ of Imidazolium ring), 838 (*vs.*, sh, PF_6), 743 (s, sh), 674 (m, sh), 559 (s, sh, P–F). ^{1}H NMR (200 MHz, DMSO-d$_6$) δ (ppm): 11.17 (s, 1H, Ar-O**H**), 9.83 (s, 1H, Ar-**H**C=O), 9.32 (s, 1H, Im-**H**), 7.84 (d, J = 2.4 Hz, 1H, Im-**H**), 7.73 (dd, J = 11.9, 1.9 Hz, 2H, Im-**H** and Ar-**H**), 7.40 (dd, J = 8.3, 2.2 Hz, 1H,

Ar-**H**), 5.36 (s, 2H, N3-C**H**$_2$-Ar), 4.17 (q, J = 7.2 Hz, 2H, N1-C**H**$_2$CH$_3$), 1.37 (t, J = 7.3 Hz, 3H, N1-CH$_2$C**H**$_3$), 1.32 (s, 9H, C(CH$_3$)$_3$). ^{13}C NMR (125 MHz, DMSO-d$_6$) δ (ppm): 193.44, 158.11, 142.01, 138.03, 135.97, 130.89, 129.37, 128.21, 123.67, 122.93, 54.92, 41.91, 27.29, 23.13, 15.26. ESI-MS: in positive mode peaks at m/z 287.4 ([$C_{17}H_{23}N_2O_2$, M–PF_6^-]$^+$) a.m.u.

2.4. 3-(3-((2-carbamothioylhydrazineylidene)methyl)-4-hydroxy-5-*tert*-butyl benzyl)-1-ethylimidazolium salts (4a–c)

Initially, a clear solution was made by warming 1 g (8.97 mmol) thiosemicarbazide hydrochloride and 0.9 g (10.97 mmol) anhydrous sodium acetate in 5 mL of distilled water. After that, a 10 mL ethanolic solution containing 6.57 mmol of imidazolium ionic liquids (**3a–c**) was added to the mixture while it was being stirred at RT. Finally, the mixture was cooled, and the formed solid was filtered out, washed thoroughly with distilled water, and dried overnight. After being recrystallized from ethanol, refiltered, and vacuum-dried, the pure products were ready for use for the following reactions. The collected samples were analyzed for their physicochemical properties, and the results are detailed below:

4a; obtained as a faint yellow powder, Yield: 81%, mp: 135 °C. FTIR (KBr, cm^{-1}): 3458 (m, br), 3285 (m, sh), 3169 (m, sh), 3169 (m, sh), 3113 (m, sh), 2959 (m, sh), 1635 (s, sh), 1560, 1453, 1351 (s, sh), 1272 (s, sh), 1165 (s, sh), 990 (m, sh), 803 (m, sh). ^{1}H NMR (300 MHz, DMSO-d_6) δ (ppm): 11.82 (s, 1H), 10.98 (s, 1H), 9.42 (s, 1H), 8.95 (s, 1H), 7.81–7.63 (m, 2H), 7.61–7.50 (m, 1H), 7.14 (s, 1H), 6.75 (s, br, 2H), 5.59 (s, 2H), 4.36 (q, J = 7.4 Hz, 2H), 1.57 (t, J = 7.3 Hz, 3H), 1.33 (s, 9H). ESI-MS: a positive mode peak at m/z = 360.3 a.m.u. corresponding to [$C_{18}H_{26}N_5OS$, M–Cl^-]$^+$.

4b; obtained as a yellow powder, Yield: 72%, mp: 141 °C. FTIR (KBr, cm^{-1}): 3429 (m, br), 3312 (m, sh), 3199 (m, sh), 3130 (m, sh), 3067 (m, sh), 2958 (m, sh), 1628 (s, sh), 1559, 1462, 1380 (s, sh), 1270 (s, sh), 1154 (s, sh), 1051 (*vs.*, sh), 996 (m, sh), 801 (m, sh), 747 (m, sh). ^{1}H NMR (300 MHz, DMSO-d_6) δ 11.87 (s, 1H), 10.91 (s, 1H), 10.01 (s, 1H), 9.31 (s, 1H), 7.87–7.65 (m, 2H), 7.47–7.35 (m, 1H), 7.18 (s, 1H), 6.68 (s, br, 2H), 5.49 (s, 2H), 4.20 (q, J = 7.2 Hz, 2H), 1.44 (t, J = 7.2 Hz, 3H), 1.31 (s, 9H). ESI-MS: a positive mode peak at m/z = 360.3 a.m.u. corresponding to [$C_{18}H_{26}N_5OS$, M–BF_4^-]$^+$.

4c; obtained as a pale yellow powder, Yield: 76%, mp: 153 °C. FTIR (KBr, cm^{-1}): 3455 (m, sh), 3284 (m, sh), 3167 (m, sh), 3109 (m, sh), 2959 (m, sh), 1635 (s, sh), 1560, 1453, 1349 (s, sh), 1271 (s, sh), 1159 (s, sh), 1030 (s, sh), 839 (*vs.*, sh), 741 (m, sh). ^{1}H NMR (300 MHz, DMSO-d_6) δ 11.91 (s, 1H), 10.88 (s, 1H), 9.97 (s, 1H), 9.16 (s, 1H), 7.85 (d, J = 2.3 Hz, 1H), 7.76–7.53 (m, 2H), 7.19 (s, 1H), 6.65 (s, br, 2H), 5.38 (s, 2H), 4.17 (q, J = 7.1 Hz, 2H), 1.39 (t, J = 7.3 Hz, 3H), 1.33 (s, 9H). ESI-MS: a positive mode peak at m/z = 360.3 a.m.u. corresponding to [$C_{18}H_{26}N_5OS$, M–PF_6^-]$^+$.

2.5. Synthesis of 1-ethyl-3-(4-hydroxy-3-*tert*-butyl-5-(((thiohydantoin-1-yl)imino)methyl) benzyl)-imidazolium salts or imidazoluim-thiohydantoins (IMTHs, 5a–c)

An ethanolic solution (20 mL) of thiosemicarbazones (**4a–c**) (5.12 mmol) in dry ethanol was treated with ethyl chloroacetate (0.62 mL, 5.11 mmol) using fused sodium acetate (0.75 g, 9.14 mmol) as a catalyst. The reaction mixture was then heated at a reflux temperature with continuous stirring for 5 h. The progress of the reaction was monitored using thin layer chromatography (TLC). When the reaction was completed, the reaction mixture was cooled down to the ambient temperature and diluted with an ice-water mixture to get the intended products. Pure IMTHs (**5a–c**) were obtained by filtering the formed solids, washing them with cold ethanol, drying them, and then recrystallizing them from hot ethanol. The obtained samples were analyzed for the following physicochemical characteristics:

IMTH$_1$, **(5a)**; pale yellow powder, Yield: 69%, mp: 168 °C. FTIR (KBr, cm^{-1}): 3443 (s, br, ν_{O-H}), 3132 (m, sh, ν_{N-H}), 3069 (m, sh, aromatic ν_{C-H}), 2960 (s, sh, aliphatic ν_{C-H}), 2588 (m, sh, ν_{S-H}), 1735 (*vs.*, sh, $\nu_{C=O}$), 1630 (s, sh, $\nu_{C=N}$), 1549 (s, sh, thioamide I, $\delta_{(N-H)}$ + $\nu_{(C-N)}$), 1464 (s, sh), 1381 (s, sh), 1272 (s, sh, ν_{Ar-O}), 1168 (s, sh, thioamide IV, $\nu_{C=S}$), 1156 (s, sh, $\nu_{(H-C=C+H-C=N)bend}$ of Imidazolium ring), 997 (m, sh), 861 (*vs.*, sh), 802 (m, sh, δ_{C-S-H}), 748 (m, sh, $\delta_{C=S}$), 621 (m, sh, δ_{C-S}). ^{1}H NMR (300 MHz, DMSO-d_6) δ (ppm): 14.02 (s, 1H, Ar-O**H**), 9.19 (s, 1H, **H**C=N), 8.53 (s, 1H, Im-**H**), 7.77 (dt, J = 15.3, 1.9 Hz, 2H, Im-**H**), 7.36 (d, J = 2.2 Hz, 1H, Ar-**H**), 7.29 (d, J = 2.2 Hz, 1H, Ar-**H**), 5.27 (s, 2H, N3-C**H**$_2$-Ar), 4.17 (q, J = 7.3 Hz, 2H, N1-C**H**$_2$CH$_3$), 2.24 (s, 2H, CH$_2$ of thiohydantoin ring), 1.86 (s, 1H, S**H**), 1.40 (t, J = 7.3 Hz, 3H, N1-CH$_2$CH$_3$), 1.24 (s, 9H, C(CH$_3$)$_3$). ^{13}C NMR (151 MHz, DMSO-d_6) δ 175.04, 160.72, 153.19, 144.69, 137.65, 134.42, 132.01, 129.96, 123.92, 122.93, 121.21, 118.53, 56.45, 50.78, 35.14, 34.88, 29.40, 9.83. ESI-MS: a positive mode peak at m/z = 400.4 a.m.u. corresponding to [$C_{20}H_{26}N_5O_2S$, M–Cl^-]$^+$. Anal. Calcd for $C_{20}H_{26}ClN_5O_2S$ (M = 435.97 g mol^{-1}): C, 55.10; H, 6.01; N, 16.06; S, 7.35%. Found: C, 55.07; H, 6.05; N, 15.97; S, 7.28%.

IMTH$_2$, **(5b)**; dark yellow powder, Yield: 71%, mp: 197 °C. FTIR (KBr, cm^{-1}): 3460 (s, br, ν_{O-H}), 3287 (s, br, ν_{N-H}), 3116 (m, sh, aromatic ν_{C-H}), 2962 (s, sh, aliphatic ν_{C-H}), 2587 (m, sh, ν_{S-H}), 1733 (*vs.*, sh, $\nu_{C=O}$), 1638 (s, sh, $\nu_{C=N}$), 1562 (s, sh, thioamide I, $\delta_{(N-H)}$ + $\nu_{(C-N)}$), 1467 (s, sh), 1352 (s, sh), 1273 (s, sh, ν_{Ar-O}), 1168 (s, sh, thioamide IV, $\nu_{C=S}$), 1155 (m, sh, $\nu_{(H-C=C+H-C=N)bend}$ of Imidazolium ring), 1058 (*vs.*, sh, $\nu_{(BF_4)}$), 992 (m, sh), 803 (m, sh, δ_{C-S-H}), 742 (m, sh, $\delta_{C=S}$), 643 (m, sh, $\nu_{(C-S)}$). ^{1}H NMR (300 MHz, DMSO-d_6) δ (ppm): 14.03 (s, 1H, Ar-O**H**), 9.20 (s, 1H, **H**C=N), 8.54 (s, 1H, Im-**H**), 7.78 (dt, J = 6.4, 1.9 Hz, 2H, Im-**H**), 7.34 (dd, J = 14.9, 2.2 Hz, 2H, Ar-**H**), 5.28 (s, 2H, N3-C**H**$_2$-Ar), 4.19 (q, J = 7.2 Hz, 2H, N1-C**H**$_2$CH$_3$), 2.26 (s, 2H, CH$_2$ of thiohydantoin ring), 1.85 (s, 1H, S**H**), 1.42 (t, J = 7.3 Hz, 3H, N1-CH$_2$CH$_3$), 1.23 (s, 9H, C(CH$_3$)$_3$). ^{13}C NMR (151 MHz, DMSO-d_6) δ 174.90, 160.28, 153.98, 144.94, 138.51, 134.39, 131.97, 125.95, 123.08, 121.32, 121.08, 118.54, 56.49, 50.31, 35.17, 34.96, 29.34, 9.87.^{11}B NMR (96 MHz, DMSO-d_6) singlet at δ −1.30 ppm. ^{19}F NMR (282 MHz, DMSO-d_6) singlet at δ −148.26 ppm. ESI-MS: a positive mode peak at m/z = 400.4 a.m.u. corresponding to [$C_{20}H_{26}N_5O_2S$, M–BF_4^-]$^+$. Anal. Calcd for $C_{20}H_{26}BF_4N_5O_2S$ (M = 487.32 g mol^{-1}): C, 49.29; H, 5.38; N, 14.37; S, 6.58%. Found: C, 49.14; H, 5.42; N, 14.29; S, 6.51%.

IMTH$_3$, **(5c)**; yellow powder, Yield: 73%, mp: 189 °C. FTIR (KBr, cm^{-1}): 3442 (s, br, ν_{O-H}), 3163 (m, sh, ν_{N-H}), 3107 (m, sh, aromatic ν_{C-H}), 2964 (s, sh, aliphatic ν_{C-H}), 2587 (m, sh, ν_{S-H}),

1734 (*vs.*, sh, $\nu_{C=O}$), 1633 (s, sh, $\nu_{C=N}$), 1541 (s, sh, thioamide I, $\delta_{(N-H)} + \nu_{(C-N)}$), 1471 (s, sh), 1349 (s, sh), 1273 (s, sh, ν_{Ar-O}), 1167 (s, sh, thioamide IV, $\nu_{C=S}$), 1155 (s, sh, $\nu_{(H-C=C+H-C=N)bend}$ of Imidazolium ring), 979 (m, sh), 901 (m, sh, δ_{C-S-H}), 837 (*vs.*, sh, $\nu_{(PF6)}$), 802 (m, sh, δ_{C-S-H}), 743 (m, sh, $\delta_{C=S}$), 620 (m, sh, δ_{C-S}), 557 (s, sh, ν_{P-F}). ^{1}H NMR (300 MHz, DMSO-d_6) δ (ppm): 14.39 (s, 1H, Ar-O**H**), 9.21 (s, 1H, **H**C=N), 8.53 (s, 1H, Im-**H**), 7.65 (dt, J = 6.4, 1.9 Hz, 2H, Im-**H**), 7.27 (dd, J = 14.9, 2.2 Hz, 2H, Ar-**H**), 5.27 (s, 2H, N3-C**H$_2$**-Ar), 4.22 (q, J = 7.2 Hz, 2H, N1-C**H$_2$**CH$_3$), 2.27 (s, 2H, CH_2 of thiohydantoin ring), 1.85 (s, 1H, S**H**), 1.45 (t, J = 7.3 Hz, 3H, N1-CH_2**CH_3**), 1.34 (s, 9H, C(**CH_3**)$_3$). ^{13}C NMR (151 MHz, DMSO-d_6) δ 175.48, 160.51, 153.05, 145.60, 136.59, 135.86, 133.30, 129.99, 129.84, 127.83, 124.63, 122.75, 57.32, 50.41, 35.65, 34.42, 30.05, 9.88.^{31}P NMR (202 MHz, DMSO-d_6): −142.96 (hept, J_{P-F} = 711.3 Hz). ^{19}F NMR (471 MHz, DMSO-d_6): −70.57 ppm (doublet, J_{F-P} = 711.3 Hz). ESI-MS: a positive mode peak at m/z = 400.4 a.m.u. corresponding to $[C_{20}H_{26}N_5O_2S, M-PF_6^-]^+$. Anal. Calcd for $C_{20}H_{26}F_6N_5O_2PS$ (M = 545.49 g mol^{-1}): C, 44.04; H, 4.80; N, 12.84; S, 5.88%. Found: C, 43.98; H, 4.82; N, 12.81; S, 5.76%.

2.6. Preparation of IMTHs complexes (6a–c)

Mn(III)IILTH complexes (**6a–c**) were prepared using a standard procedure a general protocol. Briefly, 0.9 mmol of IMTHs ligands (**5a–c**) were dissolved in anhydrous ethanol (20 mL) and then degassed under vacuum for 15 min. Thereafter, 5 mL of an ethanolic solution containing 1.1 mmol (269 mg) of $Mn(OAc)_2 \cdot 4H_2O$ was dropped into the ligand solution while stirring at room temperature in an inert N_2 environment. The yellow colour of the ligand solution quickly became dark brown, indicating complex formation. After that, the reaction mixture was heated under reflux with stirring and an N_2 atmosphere for 2 h. For the oxidation of Mn(II) into Mn(III), 69.9 mg (1.65 mmol) of LiCl was added to the Mn(II)-IMTH solution while it was being bubbled with air. The mixture was then refluxed for another 2 h. After the solvent had been evaporated partially, the remaining substance was chilled in the fridge overnight to allow precipitation of the intended complexes. Eventually, filtration was used to collect the formed solids, which were then washed with cold ethanol (2 × 3 mL), ethyl acetate (3 × 3 mL), diethyl ether (3 × 3 mL), and vacuum-dried to yield pure [Mn(III)(IMTH)(H_2O)Cl]·$x H_2O$ complexes. The obtained complexes were analyzed for the following physicochemical characteristics:

[Mn($IMTH_1$)(H_2O)Cl]·H_2O (**6a**): faint brown powder (63%). FTIR (KBr, cm^{-1}): 3433 (s, br, ν_{O-H}), 3112 (m, sh, aromatic ν_{C-H}), 2947 (s, sh, aliphatic ν_{C-H}), 1734 (*vs.*, sh, $\nu_{C=O}$), 1618 (s, sh, $\nu_{C=N}$), 1576 (s, sh, imidazoline $\nu_{(C=N)}$), 1439 (s, sh), 1386 (s, sh), 1281 (s, sh, ν_{Ar-O}), 1158 (s, sh, $\nu_{(H-C=C+H-C=N)bend}$ of Imidazolium ring), 997 (m, sh), 861 (*vs.*, sh), 642 (m, sh, δ_{C-S}), 625 (w, br, $\nu_{(Mn-O)}$), 575 (m, sh, $\nu_{(Mn-N)}$). ESI-MS: a positive mode peak at m/z = 506.7 a.m.u. corresponding to $[C_{20}H_{28}ClMnN_5O_4S, M-Cl^-]^+$. Anal. Calcd for $C_{20}H_{28}Cl_2MnN_5O_4S$ (M = 560.37 g mol^{-1}): C, C, 42.87; H, 5.04; N, 12.50; S, 5.72%. Found: C, 42.74; H, 5.07; N, 12.47; S, 5.69%.

[Mn($IMTH_2$)(H_2O)Cl]·H_2O (**6b**): brown powder (62%). FTIR (KBr, cm^{-1}): 3431 (s, br, ν_{O-H}), 3131 (m, sh, aromatic ν_{C-H}), 2955 (s, sh, aliphatic ν_{C-H}), 1731 (*vs.*, sh, $\nu_{C=O}$), 1617 (s, sh, $\nu_{C=N}$), 1576 (s, sh, imidazoline $\nu_{(C=N)}$), 1439 (s, sh), 1388 (s, sh), 1283 (s, sh, ν_{Ar-O}), 1154 (m, sh, $\nu_{(H-C=C+H-C=N)bend}$ of Imidazolium ring), 1057 (*vs.*, sh, $\nu_{(BF4)}$), 992 (m, sh), 667 (m, sh, $\nu_{(C-S)}$), 623 (w, br, $\nu_{(Mn-O)}$), 570 (m, sh, $\nu_{(Mn-N)}$). ESI-MS: a positive mode peak at m/z = 506.7 a.m.u. corresponding to $[C_{20}H_{28}ClMnN_5O_4S, M-BF_4^-]^+$. Anal. Calcd for $C_{20}H_{28}BClF_4MnN_5O_4S$ (M = 611.73 g mol^{-1}): C, 39.27; H, 4.61; N, 11.45; S, 5.24%. Found: C, 39.24; H, 4.58; N, 11.43; S, 5.19%.

[Mn($IMTH_3$)(H_2O)Cl]·H_2O (**6c**): deep brown powder (59%). FTIR (KBr, cm^{-1}): 3435 (s, br, ν_{O-H}), 3105 (m, sh, aromatic ν_{C-H}), 2948 (s, sh, aliphatic ν_{C-H}), 1732 (*vs.*, sh, $\nu_{C=O}$), 1618 (s, sh, $\nu_{C=N}$), 1441 (s, sh), 1387 (s, sh), 1285 (s, sh, ν_{Ar-O}), 1576 (s, sh, imidazoline $\nu_{(C=N)}$), 1156 (s, sh, $\nu_{(H-C=C+H-C=N)bend}$ of Imidazolium ring), 979 (m, sh), 839 (*vs.*, sh, $\nu_{(PF6)}$), 643 (m, sh, δ_{C-S}), 624 (w, br, $\nu_{(Mn-O)}$), 556 (s, sh, ν_{P-F}), 573 (m, sh, $\nu_{(Mn-N)}$). ESI-MS: a positive mode peak at m/z = 506.7 a.m.u. corresponding to $[C_{20}H_{28}ClMnN_5O_4S, M-PF_6^-]^+$. Anal. Calcd for $C_{20}H_{28}ClF_6MnN_5O_4PS$ (M = 669.89 g mol^{-1}): C, 35.86; H, 4.21; N, 10.45; S, 4.79%. Found: C, 35.81; H, 4.27; N, 10.42; S, 4.72%.

2.7. Biological studies

2.7.1. *In vitro* antimicrobial assay. The antimicrobial potency of newly synthesized imidazolium-thiohydantoin hybrids (IMTHs) and their Mn(III) complexes was tested *in vitro* against the most common foodborne ESKAPE pathogens (*S. aureus* (ATCC-29737), *S. pneumoniae* (ATCC-49619), *E. coli* (ATCC-10536), *P. aeruginosa* (ATCC-27853), *K. pneumonia* (ATCC-13883)). Amoxicillin, Tetracycline, and Gentamycin were used as positive controls. All bacterial strains were generously supplied by the NODCAR in Cairo, Egypt, and were routinely grown on nutrient broth agar (NBA). The starter bacterial culture was freshly prepared by inoculating Mueller Hinton Broth (MHB) with a bacterial suspension containing ~10^6 CFU mL^{-1} and incubating it at 37 °C and 5% CO_2 atmosphere. The sensitivity of bacterial strains toward the new compounds was initially investigated using disk diffusion assay as described in our earlier work.[35] The primary indicators for the antibacterial capabilities of the investigated compounds were the values of the diameters of the inhibition zone (DIZ, mm). Each experiment was performed in triplicates, and the mean ± SEM data were used to determine antibacterial efficacy.

2.7.1.1. MIC and MBC assay. The antibacterial effectiveness indices, minimal inhibitory concentration (MIC) and minimal bactericidal concentration (MBC), of novel compounds and antibiotics against tested bacterial strains, were evaluated using the microtitre broth dilution technique as prescribed in our earlier work.[36] Briefly, compounds and antibiotics were dissolved in DMSO and diluted in Mueller–Hinton Broth (MHB) before being added to the bacterial suspension. Then, 190 μL of the bacterial samples (~10^6 CFU mL^{-1}) were transferred to 96-well microtiter plates, followed by the addition of the serially diluted compounds and antibiotics ranging in concentration from 0.25 mM to 50.0 mM and they were incubated at 37 °C for 24 h; at the same time, untreated wells were served as controls. MIC and MBC values were determined by checking the turbidity

of wells. Multiple independent replicates of each sample were tested in order to determine the MIC and MBC. The findings have been expressed as the mean ± SEM.

2.8.1. *In vitro* cytotoxicity assay

2.8.1.1. Cell cultures. This study compared the cytotoxicity styles of novel substances on the human liver hepatocellular carcinoma (Hepg2) and healthy human liver (HL7702) cell lines. The Egyptian VACSERA tissue culture facility generously supplied these cell lines. These cell lines were grown in the Roswell Park Memorial Institute 1640 (RPMI-1640) growth medium supplemented with 10% thermally-deactivated foetal bovine serum (FBS, HyClone, Thermo Scientific), L-glutamine (1%), and gentamycin (100 μg mL^{-1}) (HyClone, Thermo Scientific), and 4-(2-hydroxyethyl)-1-piperazineethanesulfonic acid (HEPES) buffer. Afterwards, the cell cultures were incubated for 24 h at 37 °C in a 5% humidified CO_2 atmosphere.

2.8.1.2. In vitro anti-proliferative activity. An MTT test was used to assess the survival of Hepg2 and HL7702 cell lines treated with the most efficient antibacterial agents.[37] In brief, 200 μL of each cell line was transferred to a 96-wells plate (2.3×10^5 cells/well) and treated with serially diluted samples (0.25–100 μM) and Vinblastine (VBL) as a positive control. DMSO was served as a negative control. The wells were categorized into sets, consisting of three wells per sample. After incubation of the test plate at 37 °C in a 5% CO_2 atmosphere for 48 h, 20 μL of MTT reagent (5 mg mL^{-1} in a 0.9% NaCl solution) was added to each well and then the plate was re-incubated for an additional 4 h. After that, the residual staining reagent (MTT) was carefully discarded, and the produced formazan crystals were solubilized by adding acidified isopropanol (180 μL per well) while continuously shaking using a MaxQ 2000 plate shaker (Thermo Fisher Scientific Inc., MI, USA). The survivor cells was estimated spectrophotometrically by recoding the absorbance at 570 nm using a Stat FaxR 4200 plate reader. Values of Mean ± S.E were used to express the surviving fractions. The surviving fractions were expressed using mean ± SEM values.

2.9. Statistical analyses

The independent Student's *t*-tests in SPSS v17 and OriginPro 9.1 32 were used to handle the findings of this study and extract results as well as graphs. The significance threshold was set at $P < 0.05$, and all data were shown as the mean ± standard medium error.

3. Results and discussion

3.1. Chemistry

The main precursors for this work, *tert*-butylsalicylaldehyde-ethylimidazolium (TBSEIM) salts (**3a–c**), were synthesized from 2-*tert*butylphenol using a slightly modified version of our previously published protocol. Initially, *ortho*-formylation of 2-*tert*-butylphenol under ultra-dry conditions with paraformaldehyde catalyzed by anhydrous $MgCl_2$ as the *O*-magnesiation reagent and triethylamine gave 3-*tert*-butylsalicylaldehyde (TBS, **1**), which was then chloromethylated to get 5-chloromethyl-3-*tert*butylsalicylaldehyde (CMTBS, **2**) using paraformaldehyde/$ZnCl_2$/HCl as a chloromethylating mixture (see Scheme 1). Subsequently, tert-butylsalicylaldehyde-ethylimidazolium chloride (**3a**) was synthesized through quaternization of 1-ethylimidazole with CMTBS, and its tetrafluoroborate and hexafluorophosphate analogs (**3b** and **3c**) were prepared *via* reactions with $NaBF_4$ and KPF_6, respectively. After that, thiosemicarbazones **4a–c** are formed through the Schiff-base condensation of TBSEIM salts (**3a–c**) with thiosemicarbazide in an acidic medium. Reacting these thiosemicarbazones with ethyl chloroacetate in the presence of a catalytic quantity of fused CH_3COONa yielded the corresponding imidazoluim-thiohydantoins (IMTHs, **5a–c**). The thiohydantoins were produced with extremely high yields and purities that were unparalleled. On the other hand, using a one-pot, two-step preparation process, the chlorido Mn(III)IMTH complexes (**6a–c**) were synthesized. In the first step, in an N2 atmosphere, the acetate groups in $Mn(OAc)_2 \cdot 4H_2O$ have readily swapped with IMTHs. After that, the flow of oxygen into the reaction medium made it possible for the Mn(II) core to spontaneously oxidize into Mn(III) species. This was followed by the coordination of Mn(III) ion with chloride ion that was released from LiCl.[38] Unfortunately, despite extensive efforts, we could not obtain single crystals of Mn(III)IMTH complexes qualified enough for X-ray measurements. Thus, the structural characteristics of novel complexes were suggested using elemental (CHNS), spectroscopic (FTIR, UV-vis, ESI-MS), and magnetic studies.

3.2. Structural characterization

3.2.1. FTIR. For any novel complexes, FTIR spectroscopy should serve as the initial instructive guide to verify their effective creation and investigate their interior coordination modes.[39] First, the primary distinctive IR peaks of the native imidazolium-thiohydantoin ligands (IMTHs, **5a–c**) were identified by inspection of their FTIR spectra (Fig. 1A). The absorption peaks at approximately 3450 $^{-1}$ (phenolic OH group), 3130 cm^{-1} (N–H group), and 1635 cm^{-1} (azomethine group) appear as the major IR-spectral signatures of IMTHs. Moreover, two different sets of absorption bands can be seen in the IMTHs spectra. The first set of peaks was observed at approximately 1734 cm^{-1} (carbonyl, C=O), 1168 cm^{-1}, (thioamide IV, N–C=S), 1562 and 1545 cm^{-1} (thioamide I, $\delta_{(N-H)} + \nu_{(C-N)}$). This set could be assigned to the vibrational modes of the thione tautomeric form of the thiohydantoin ring. The other group of peaks, detected at around 2587, 802, 643 cm^{-1} and assigned to the S–H, C–S–H, and C–S groups, respectively, is characteristic of the thiol form of the thiohydantoin meioty.[35] The variation seen in the spectra of Mn(III)IMTHs when compared to their free ligands confirms their successful synthesis.[40] For example, the disappearance of the phenolic OH stretch and the red-shifting of the aryl-O peak by 11 cm^{-1} are suggestive of phenolic OH group deprotonation and subsequent coordination of the generated phenolate anion with Mn(III) ion. Our hypothesis is supported by the appearance of additional peaks in the FTIR spectra of complexes around 624 cm^{-1}, which are typical of Mn–O.[41] Similarly, the disappearance of the IR peaks of the thiol (S–H) and thione (C=S) groups, as well as negative shifts in the C–S peaks, are indicative of the deprotonation of the thiol group of the thiohydantoin ring and

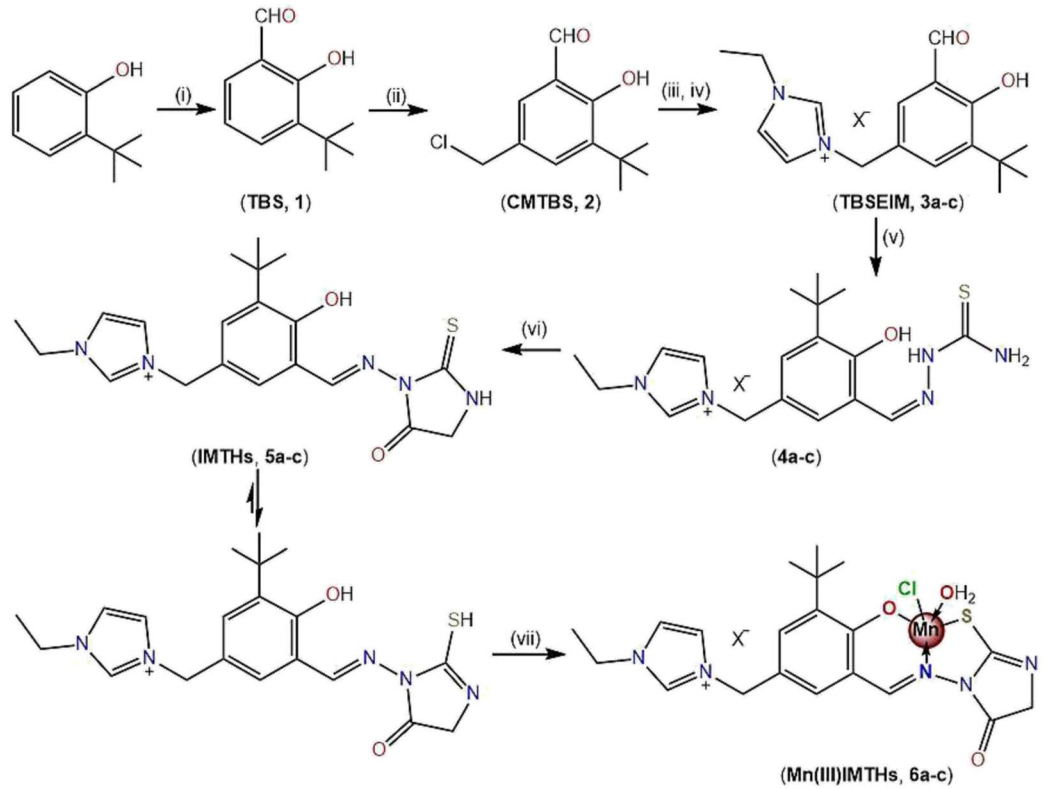

Scheme 1 Step by step synthesis of imidazoluim-thiohydantoins (IMTHs, **5a–c**) and their Mn(III) complexes (Mn(III)IMTHs, **6a–c**).

involvement of the resulting thiolate anion in the coordination environment of Mn ion. Meanwhile, the emergence of a new weak absorption band in the range of 613 ± 2 cm^{-1}, which is typical for Mn–S,[42] confirms our suggestion. Additionally, the involvement of azomethinic-N in the coordination sphere of Mn ion is revealed by a negative shift of 12–16 cm^{-1} in the azomethine absorption band of the free IMTH ligands.[43]

Conversely, during complex formation, there is almost no change in the strength or location of the carbonyl IR peak, which rules out carbonyl group sharing during the complexation event. These findings revealed that the IMTH ligands serve as dianionic tridentate (ONS) ligands. The existence of water molecules within the coordination sphere of Mn(III) ion was verified by the emergence of new wide bands at the regions

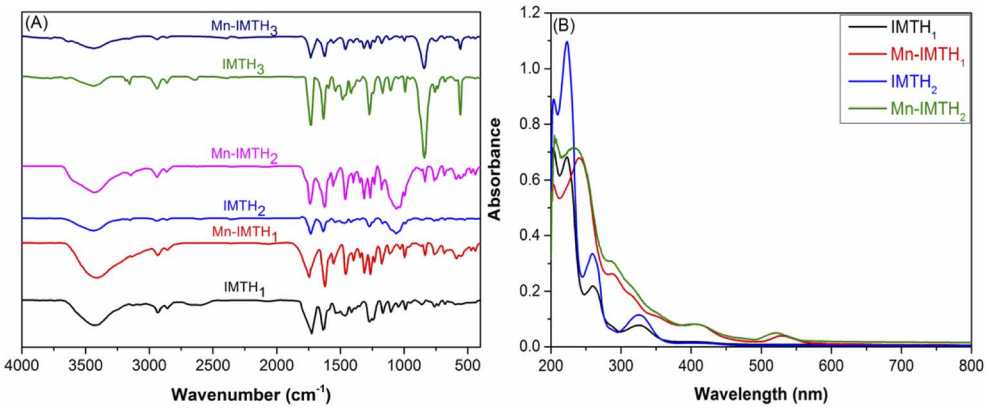

Fig. 1 (A) FTIR spectra of the free IMTH ligands and their complexes (Mn(III)IMTHs). (B) UV-vis spectra for the ethanolic solutions (10^{-3} M) of the free IMTH ligands and their complexes (Mn(III)IMTHs).

Table 1 UV-vis peaks (λ_{max}, nm) and their assignments as well as the magnetic moments (B.M) for the IMTH ligands and their Mn(III)-complexes

	Electronic transitions			
Compound	$\pi \rightarrow \pi^*$	$n \rightarrow \pi^*$	$p\pi \rightarrow d\pi^*$, $d \rightarrow d$	μ_{eff} B.M
$IMTH_1$ (**5a**)	225, 262	326	—	—
$[Mn(III)(IMTH_1)Cl(H_2O)]$ (**6a**)	239, 281	401	521	4.87
$IMTH_2$ (**5b**)	226, 259	325	—	—
$[Mn(III)(IMTH_2)Cl(H_2O)]$ (**6b**)	237, 280	292, 402	522	4.89
$IMTH_3$ (**5c**)	227, 263	329	—	—
$[Mn(III)(IMTH_3)Cl(H_2O)]$ (**6c**)	236, 283	401	523	4.93

around 3433, 750, and 660 cm^{-1} attributed to $\nu_{(OH)}$, $\rho r_{(H_2O)}$, and $\rho w_{(H_2O)}$ vibrations, respectively.

3.2.2. UV-vis spectra. The UV-vis spectra of the IMTH ligands and their Mn(III)-complexes were examined in ethanol, and the results of this investigation, as well as the spectral peak assignments, are shown in Fig. 1B and Table 1. The three dominant peaks in the free ligand spectra, at 226 ± 1, 261 ± 2, and 327 ± 2 nm, may be attributed to the $\pi \rightarrow \pi^*$ and $n \rightarrow \pi^*$ electronic transitions of the heterocyclic/phenyl moieties and electron-rich groups (C=O, C=S, and HC=N), respectively.[15,44] When the electronic spectra of the Mn(III)IMTH complexes are compared to those of the free IMTH ligands, the major peaks show bathochromism and hypochromicity, confirming the binding of these ligands to the Mn(III) ion. For instance, the azomethine peak (327 nm) has relocated to around 400 nm, and its intensity was greatly reduced. These results lend credence to our hypothesis that the observed change in the $n \rightarrow \pi^*$ transition is due to the coordination of the ligand to the Mn(III) ion. Interestingly, the appearance of new broad absorption bands in the complex spectra at 522 ± 1 nm could be attributed to the three permissible d–d transitions (($d_{xz} \rightarrow d_{x^2-y^2}$), ($d_{xy} \rightarrow d_{x^2-y^2}$), and ($d_{z^2} \rightarrow d_{x^2-y^2}$)), which are highly indicative of the square-pyramidal geometry of these complexes.[45] The complex magnetic moment values (4.87–4.93 μ_B) also provide additional evidence for the square pyramidal structure that contains a high spin metal center.[38]

3.2.3. NMR spectroscopy. NMR spectroscopy is a powerful technique for studying the tautomeric equilibria between the thiol (T_{SH}) and thione (T_{NH}) forms of novel thiohydantoins, as well as the relative contributions of these two forms.[46,47] Since all IMTH ligands have the same organic cation and consequently identical $^1H/^{13}C$ NMR spectra, therefore, the ^1H NMR spectrum of $IMTH_2$ (**5b**) (Fig. 2A), as a representative of all ligands, was extensively studied. The two singlets observed in the low-field region at δ of 14.03 and 9.20 ppm could be assigned to the resonance of phenolic (Ar-O**H**) and azomethine (**H**C=N) protons, respectively. Noteworthy, a singlet NMR peak at 9.98 ppm corresponding to the proton from the thioamide (H–N–C=S) segment of the T_{NH} tautomer.[48] Conversely, the appearance of a 1.85 ppm S–H singlet peak in the deuterated solution of thiohydantoin revealed that the T_{SH} tautomer had a role in maintaining the equilibrium of the ligand's tautomers.[48] Using the NH/SH peak intensity ratio, we may deduce that the core backbone of **4b** exists in solution mostly as the thiol form (T_{SH}) (55%), with some input from the thione form (T_{NH}) (45%). Meanwhile, ^{13}C NMR spectroscopy gives more proof for the co-existence of the TSH and TNH tautomeric forms in these thiohydantoin solutions. Kobyka *et al.* reported that the ^{13}C resonance of these tautomers changes from 179 ppm, distinctive of thione groups (C=S) for a pure thione form, to 160 ppm, distinctive of thiol groups (C–S–H) for a pure thiol form.[48]

The ^{13}C NMR spectra of thiohydantoin ligands (Fig. 2) show four low-field peaks at the chemical shifts of ~179, ~175, ~160, and ~154 ppm, which can be ascribed to the resonance of carbon atoms in the thiocarbonyl (C=S), carbonyl (C=O), azomethine (HC=N), and C–S groups. For the IMTH ligands (**5b,c**), ^{11}B NMR, ^{19}F NMR, and ^{31}P NMR spectra were used to probe the structural identities of the counter-anions. For instance, the existence of BF_4 as a counter anion for this ligand is confirmed by the appearance of two singlets with chemical shifts of −1.30 and −148.26 ppm in the ^{11}B NMR and ^{19}F NMR spectra of $IMTH_2$ (**5b**), respectively. Whereas, PF_6 acts as a counter anion for ligand **4c**, as evidenced by the presence of a septet and a doublet in the corresponding ^{31}P NMR and ^{19}F NMR spectra at −143.58 and −68.43 ppm, respectively.

3.3. Pharmacological studies

3.3.1. Antibacterial performance

3.3.1.1. Well diffusion assay (WDA). The antibacterial properties of newly synthesized imidazolium-thiohydantoin hybrids (IMTHs) and their Mn(III) complexes were tested *in vitro* against the most common foodborne ESKAPE pathogens (*S. aureus* (SA), *S. pneumoniae* (SP), *E. coli* (EC), *P. aeruginosa* (PA), and *K. pneumonia* (KP)) in comparison to clinical antibiotics Amoxicillin (AMX), Tetracycline (TC), and Gentamycin (GM). The diameter of the inhibition zone (DIZ, mm) induced by the sample was used as a preliminary antibacterial efficiency indices. According to DIZ values (Fig. 3), all of the samples have the capacity to considerably reduce bacterial cell proliferation; however, their effectiveness varies by bacterium type and chemical structure. For example, as can be shown in Fig. 3A, the Gram-negative bacterial strains (EC and PA) showed greater resistance to all treatments than the Gram-positive ones (SA and SP) (Fig. 3B). This may be because the outer bacterial walls of the two types have different structural characteristics, resulting in a variable tendency of bacterial cell membrane permeability for investigated samples. When compared to Gram-positive

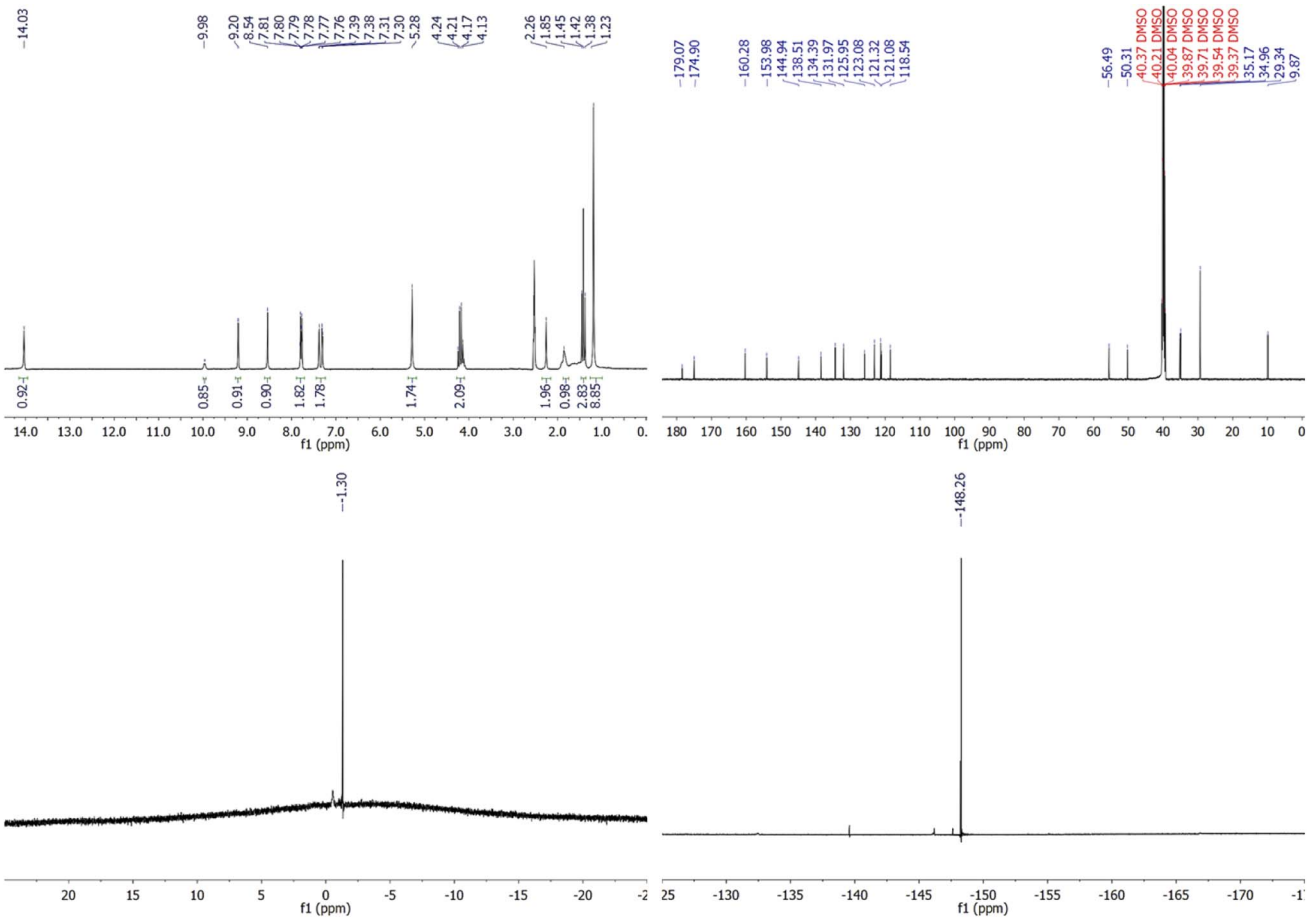

Fig. 2 ^{1}HNMR (DMSO-d_6, 200 MHz), ^{13}CNMR (DMSO-d_6, 125 MHz), ^{11}BNMR (DMSO-d_6, 96 MHz), and ^{19}FNMR (DMSO-d_6, 471 MHz) spectra of $IMTH_2$ (**5b**).

bacteria, whose outer membranes consist only of a thin peptidoglycan layer, Gram-negative bacteria's outer walls are more complex because they contain a layer of impermeable lipopolysaccharides (LPS), phospholipids (PLs), and lipoproteins (LPs), which may act as a barrier to the entry of antimicrobial agents.[49] Surprisingly, KP is the most sensitive bacterial strain for the majority of treatments. Interestingly, the antibacterial activity of IMTHs has been significantly improved following the coordination with Mn(III) ion, as revealed from their respective DIZ values. Further, it has been found that varying the counter

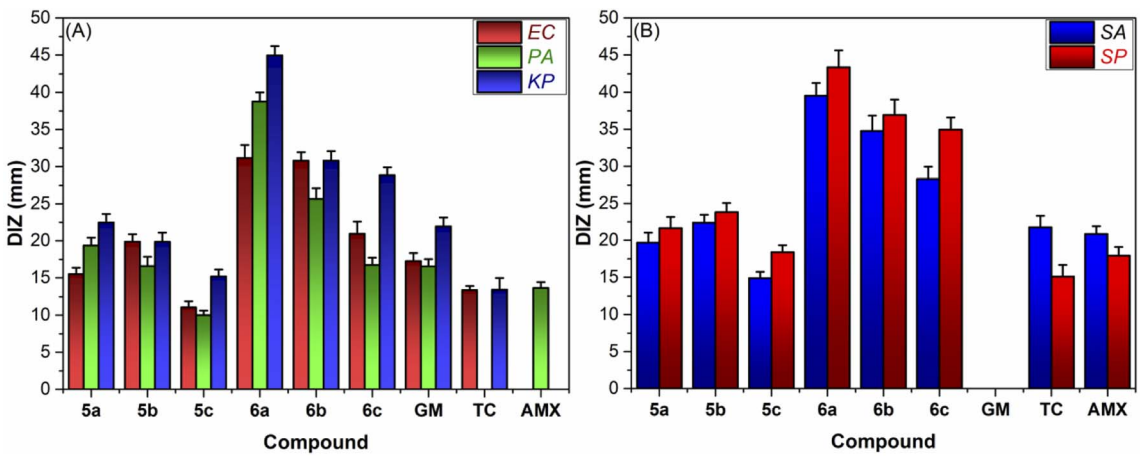

Fig. 3 Graph for the diameter of the inhibition zone (DIZ, mm) for the examined compounds against (A) Gram-negative bacteria and (B) Gram-positive bacteria.

Table 2 MIC and MBC values (mM) for the newly synthesized Mn(III)IMTHs complexes against ESKAPE pathogens, in comparison to clinical antibiotics[a]

Pathogen	Parameter	6a	6b	6c	GM	TC
SA	MIC ± SD	2.55 ± 0.25	3.07 ± 0.35	5.15 ± 0.56	NA	7.20 ± 0.66
	MBC ± SD	2.55 ± 0.27	3.19 ± 0.29	5.25 ± 0.55	NA	NA
SP	MIC ± SD	1.75 ± 0.25	2.47 ± 0.15	4.27 ± 0.35	NA	6.85 ± 0.66
	MBC ± SD	1.75 ± 0.25	2.49 ± 0.25	4.25 ± 0.42	NA	NA
EC	MIC ± SD	4.50 ± 0.28	5.25 ± 0.29	6.50 ± 0.39	6.95 ± 0.56	11.25 ± 0.75
	MBC ± SD	4.55 ± 0.32	5.35 ± 0.25	6.50 ± 0.42	NA	NA
PA	MIC ± SD	13.18 ± 0.85	18.32 ± 1.05	26.32 ± 1.18	16.74 ± 1.25	NA
	MBC ± SD	13.22 ± 0.75	18.45 ± 0.95	26.45 ± 1.15	16.74 ± 1.25	NA
KB	MIC ± SD	0.65 ± 0.15	1.25 ± 0.17	3.15 ± 0.25	8.27 ± 0.50	9.13 ± 0.56
	MBC ± SD	0.65 ± 0.16	1.25 ± 0.19	3.15 ± 0.26	NA	NA

[a] NA = not assigned.

anion dramatically alters the antibacterial efficacy of Mn(III) IMTH complexes. The most effective antibiotic (DIZ from 44.95 ± 2.11 to 31.14 ± 1.65 mm), Mn-IMTH$_1$ (**6a**), was produced by the chloride ion. Meanwhile, Mn-IMTH$_2$ (**6b**), a tetrafluoroborate-supported complex, is a more potent antibiotic than its hexafluorophosphate counterpart (see Fig. 3).

3.3.1.2. Minimal inhibitory/bactericidal concentrations (MIC/MBC). According to Table 2, the MIC and MBC findings are generally consistent with the WDA. Gram-positive bacteria, once again, are more responsive to Mn(III)IMTHs therapies (MIC/MCB = 1.75/1.75–5.15/5.25 mM) than Gram-negative bacteria (MIC/MCB = 4.50/4.55–26.32/26.45 mM), with the exception of KP (MIC/MCB = 0.65/0.65–3.15/3.15 mM). This might be explained by the presence of many negatively charged phosphate groups on its outer surface,[50] which interact strongly with the cationic imidazolium segment of Mn(III)IMTH complexes. From its MIC and MBC values (Table 2), the chloride analog stands out as the most effective antibiotic of the complexes studied (MIC/MCB ranged from 0.65/0.65 for KB to 13.18/13.22 for PA). Noteworthy, the bactericidal and bacteriostatic activity of thiohydantoin complexes based on imidazolium were diminished upon chloride exchange with other anions (BF_4^- and PF_6^-). For example, by exchanging hexafluorophosphate for chloride in Mn-IMTH$_1$ (**6a**), the resulting Mn-IMTH$_3$ (**6c**) exhibited antibacterial activity that was 1.5- to 5-times lower than that of **6a**, depending on bacterium strain. Overall, the anion metathesis significantly altered both the MIC and MBC values. These findings agree with recent reports demonstrating that the hydrophilic and chaotropic characteristics of an anion are intimately related to the antibacterial effect of ionic liquids substituted with small alkyl groups.[51] Small hydrophilic and highly chaotropic anions, like chloride and tetrafluoroborate anions, interacted strongly with water molecules and so remained in the solution, making it easy for the cation to penetrate the bacterial cell and exert its bactericidal consequences. In contrast, the hydrophobic and less chaotropic hexafluorophosphate anion did not form any stable interactions with water and thus followed the cation into the lipid bilayer, where it formed a barrier film at the phospholipid/water interface, reducing the cation's ability to enter the bacterial cell and exert its antibacterial effects.[30]

3.3.2. *In vitro* anticancer study. Many reports have demonstrated the anticancer properties of ionic liquids (ILs)-supported derivatives.[30,52] So far, no prior studies on the use of imidazolium ILs-based thiohydantoin hybrids for anticancer objectives have been reported. These findings motivated us to create and test the antiproliferative activity of novel imidazolium-thiohydantoins tethered to various anions. To that end, the most efficient antibiotics, Mn(III)IMTHs complexes, were tested *in vitro* for their anti-liver cancer capabilities against human liver carcinoma (HepG2) cells as compared to a clinical anticancer medication, vinblastine (VBL; $C_{46}H_{58}N_4O_9$, 810.99 g mol^{-1}). To verify the selectivity of novel anti-liver cancer drugs, the cytotoxicity of these complexes was also investigated in healthy liver cells (HL7702).

3.3.2.1. In vitro cytotoxicity. As can be shown in Fig. 4A, the cellular viability of HepG2 cells is drastically reduced following treatment with increasing concentrations of Mn(III)IMTHs, with performance style dependent on the structural properties of the chemotherapeutic agent and its concentration. Overall, Mn(III) IMTH$_2$ complex (**6b**), supported by tetrafluoroborate anion, was the most active anti-liver cancer agent, with the ability to decrease the number of surviving HepG2 cells from 100% to ~12% and ~3% (~88% and ~97% growth reduction) following treatment with 25 μM and 100 μM dosages, respectively. In contrast, Mn(III)IMTH$_2$ (**6c**), which contains a hydrophobic hexafluorophosphate anion, is the least cytotoxic since it reduces HepG2 viability by just ~57% and ~80% when used at the same concentrations. Our results are consistent with the general pattern of cytotoxicities for 1-alkyl-3-methylimidazolium cation [RMIM]$^+$ that has been described in the literature; [RMIM][BF_4] > [RMIM][Cl] > [RMIM][PF_6].[30] Meanwhile, the IC_{50} values confirmed that Mn(III)IMTH complexes supported by BF4 and Cl (**6b**, 1.92 ± 0.56 μM; **6a**, 5.87 ± 1.03 μM) were more efficient against liver cancer than PF6-based complexes (**6c**, 18.89 ± 1.26 μM).

3.3.2.2. Cancer cell-selectivity. The effect of increasing doses of imidazolium-thiohydantoin complexes (Mn(III)IMTHs, **6a–c**) (1.56–100 μM) on the viability of HL7702 cells after 24 h of therapy was studied to determine whether or not imidazolium-thiohydantoin complexes (Mn(III)IMTHs, **6a–c**) are selective for attacking tumor cells over healthy cells. Fig. 4B demonstrates

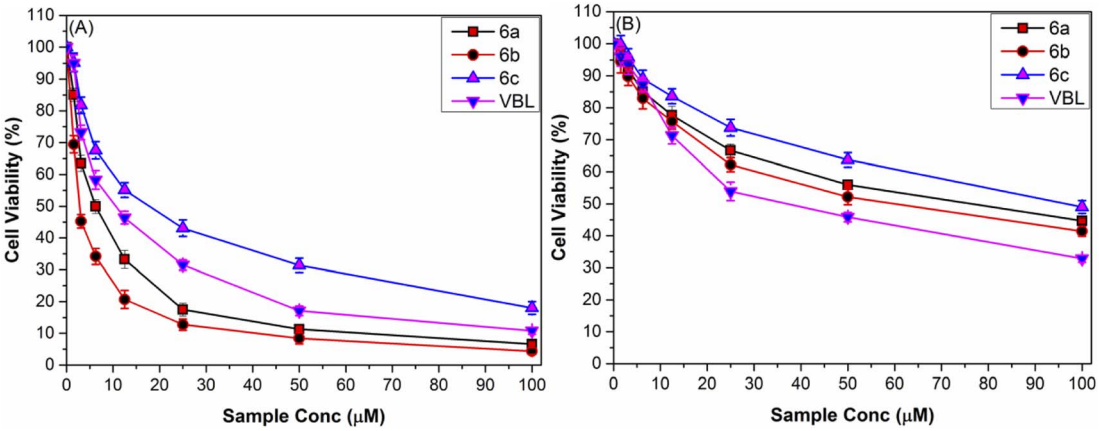

Fig. 4 Cytotoxicity-dosage graph for the Mn(III)IMTHs complexes against (A) liver carcinoma (HepG2) and (B) healthy liver cells (HL7702) in comparison to the clinical anticancer drug (VBL).

Table 3 IC_{50} (μM) and SI values for the imidazolium-thiohydantoin complexes (Mn(III)IMTHs, **6a–c**) against malignant cells (HepG2) and healthy cells (HL7702), in comparison with a clinical drug (VBL)

	IC_{50} (μM) ± SD			
Cell line	**6a**	**6b**	**6c**	VBL
HepG2	5.87 ± 1.03	1.92 ± 0.56	18.89 ± 1.26	11.46 ± 1.03
HL7702	79.63 ± 2.45	61.54 ± 2.09	89.81 ± 2.35	36.73 ± 2.52
SI	13.57	32.05	4.76	3.21

that, in contrast to their effects on cancer cells, all complexes had less of a dose-dependent impact on the viability of HL7702 cells. Interestingly, novel complexes are less toxic to healthy cells than the current drug (VBL). To measure the preference of these complexes for fighting cancerous HepG2 cells over healthy ones, the selectivity index (SI) was computed using the following formula:[53]

$$SI = \frac{IC_{50}\ \text{against healthy cells}}{IC_{50}\ \text{against cancer cells}}$$

According to the data in Table 3, we can see that the candidate (**6b**) with the highest activity against liver cancer also showed the highest selectivity (SI = 32.05) for targeting malignant cells (HepG2) over healthy cells (HL7702). Therefore, $[Mn]^{III}((IMTH_2)Cl)\cdot[BF_4]$ (**6b**) shows promise as a safe and effective anti-liver cancer therapy that does not cause damage to normal human liver cells. In light of these findings, this study paves the way for future research into potentially effective IMTH-based anti-liver cancer therapies.

3.3.3. Hydrophilicity, lipophilicity, and bioavailability of new anticancer agents. Hydrophilicity, hydration state, hydrolytic cleavage susceptibility, and hydrogen bonding capacity are all possible reasons for the anion-dependent cytotoxicity of novel imidazolium ILs-based thiohydantoin complexes.[30] The superior anticancer impact of the BF_4-based complex (**6b**) may be due to its ability to form stable ion pairs with imidazolium cation in aqueous solutions, which increases the bioavailability of the whole complex, promoting its interaction with the cancer cell membrane and generating severe cytotoxic effects.[54] Furthermore, hydrophilic anions (BF_4^- and Cl^-) can form stable hydration layers that act as a platform for active H-bonding sites (HBSs) (4F, and H in the case of BF_4 or H only in the case of Cl), whereas the hydrophobic PF_6 anion cannot form stable hydration layers and thus has a limited number of active HBSs.[30] As a result of its increased chaotropic activity, the BF_4-based complex (**6b**) can make more H-bonds with DNA nucleobases than the other counterparts (**6a** and **6c**), and therefore it can disrupt the H-bonding network in biological macromolecules (DNA and proteins).

The lipophilicity (log *P*), aqueous solubility (log *S*), and total polar surface area (TPSA) values (Table 4) are interesting because they can be used to detect the bioavailability of new anticancer agents. Generally, the new chemotherapeutic agent typically shows improved bioavailability, and low dosages of it could achieve a good clinical response when it has both a low log *P* and a high aqueous solubility value.[55] Consequently, according to the results in Table 2, **6a** and **6b** showed greater bioavailability than **6c**. Still, compared to its counterparts (**6a** and **6c**), complex (**6b**) has a greater number of H-bonding acceptor sites (HBAs), allowing it to form more H-bonds with DNA nucleobases than them and thus more effectively disrupting the H-bonding network in biological macromolecules (DNA and proteins).

Table 4 Hydrophilicity, lipophilicity, and bioavailability parameters of new anticancer agents

Compd	MW[a] (g mol^{-1})	HBD[b]	HBA[b]	log S[c]	log P[d]	TPSA (Å^2)[d]
6a	542.37	2	5	−3.788	1.562	76.95
6b	593.722	2	9	−4.939	3.353	76.95
6c	651.88	2	5	−7.478	5.436	76.95

[a] molecular weight (MW). [b] H-bonding donors/acceptors (HBD/HBA) calculated using free online ADME calculator (https://armakovic.com/online-tools/adme-calculator/). [c] aqueous solubility (log *S*) calculated using ChemDraw 16. [d] calculated using free online ADME calculator.

3.3.4. Proposed mechanism for pharmacological activity of new complexes. There is still a lot of mystery surrounding the mechanisms by which transition metal complexes cause their toxic effects on bacterial or cancer cells. However, when proposing the antibacterial or anticancer modes of action for ionic Mn complexes, the following principles should be considered: (i) the antibacterial and anticancer effects of new imidazolium-supported Mn complexes rely on their ability to firmly adhere to the phospholipid bilayers of bacterial membrane or cancer cells *via* electrostatic binding between the negative charges on the outer surfaces of bacterial or cancer cells and the positively charged imidazolium moiety. These cause the membranes in both bacterial and cancer cells to become dysfunctional and eventually cause cell death.[30] (ii) The Mn(III) ion can disrupt redox signaling in tumor and bacterial cells by promoting the oxidation of their growth factors (catecholamines), resulting in the formation of reactive oxygen species (ROS) (O_2^-, H_2O_2) and reactive quinones and semiquinones that can interact with glutathione (GSH) and deplete cellular levels. These interactions may explain manganese's toxicity.[56] (iii) In addition, Mn(III) is a hard acid, thus it aggressively interacts with the hard nitrogenous nucleobases of DNA to halt its replication, which effectively shuts down the cell's nuclear machinery.[57] Finaly, several factors, including a compound's lipophilicity, hydration state, vulnerability to hydrolytic cleavage, and hydrogen-bonding capacity, may responsible for the anion-dependent toxicity of new compounds.

4. Conclusion

In this work, we report the effective synthesis of a novel series of imidazolium-thiohydantoin hybrids (IMTHs, **5a–c**) and their Mn(III) complexes (Mn(III)IMTHs, **6a–c**), starting with 2-*tert*-butylphenol. Based on the results of spectroscopic (FTIR, UV-vis, NMR (^{1}H, ^{13}C, ^{19}F, ^{11}B) and ESI-MS) and physicochemical (elemental and magnetic) analyses, the structural aspects of hybrids and their complexes were explored, as were the coordination styles between IMTHs and Mn(III) ions. The *in vitro* antibacterial assay against ESKAPE pathogens revealed that all complexes are more effective antibiotics than their parent ligands, as indicated by their DIZ and MIC/MBC values. Furthermore, Gram-negative bacterial strains (EC and PA) were more resistant to all treatments than Gram-positive ones (SA and SP). The chloride analog (Mn-IMTH$_1$ (**6a**)) stands out as the most effective antibiotic of the complexes studied (MIC/MCB ranged from 0.65/0.65 for KB to 13.18/13.22 for PA). The MTT assay results showed that all Mn (III)IMTHs had the potential to reduce the viability of liver carcinoma (HepG2) cells in a dose-dependent manner, with the BF_4-supported complex (**6b**) outperforming its counterparts (**6a** and **6c**) as well as a clinical anticancer drug (VBL). Additionally, Mn-IMTH$_2$ (**6b**) showed the highest level of selectivity (SI = 32.05) for targeting malignant cells (HepG2) over healthy cells (HL7702). These results highlight the significance of these complexes as promising new prospects for the discovery and development of innovative chemotherapeutic drugs in the treatment of liver cancer.

Conflicts of interest

The authors declare there is no conflict of interest.

Acknowledgements

The authors extend their appreciation to the Deanship of Scientific Research at King Khalid University for funding this work through large Groups (project under grant number R.G.P.2/161/143).

References

1 A. Catalano, D. Iacopetta, J. Ceramella, D. Scumaci, F. Giuzio, C. Saturnino, S. Aquaro, C. Rosano and M. S. Sinicropi, *Molecules*, 2022, **27**, 616.
2 M. S. Mulani, E. E. Kamble, S. N. Kumkar, M. S. Tawre and K. R. Pardesi, *Front. Microbiol.*, 2019, **10**, 539.
3 S. Zhang, J. Zhang, P. Gao, L. Sun, Y. Song, D. Kang, X. Liu and P. Zhan, *Drug Discovery Today*, 2019, **24**, 805–813.
4 M. Pandey, M. Singh, K. Wasnik, S. Gupta, S. Patra, P. S. Gupta, D. Pareek, N. S. N. Chaitanya, S. Maity, A. B. M. Reddy, R. Tilak and P. Paik, *ACS Omega*, 2021, **6**, 31615–31631.
5 A. K. Yamala, V. Nadella, Y. Mastai, H. Prakash and P. Paik, *Nanoscale*, 2017, **9**, 14006–14014.
6 V. Abbot, P. Sharma, S. Dhiman, M. N. Noolvi, H. M. Patel and V. Bhardwaj, *RSC Adv.*, 2017, **7**, 28313–28349.
7 R. Gondru, Y. Li and J. Banothu, *Eur. J. Med. Chem.*, 2022, **227**, 113921.
8 J. Walsh and A. Bell, *Curr. Pharm. Des.*, 2009, **15**, 2970–2985.
9 S. Peter, S. Alven, R. B. Maseko and B. A. Aderibigbe, *Molecules*, 2022, **27**, 4478.
10 V. B. Kumar, H. Medhi, Z. Yong and P. Paik, *Nanomed.: Nanotechnol. Biol. Med.*, 2016, **12**, 579–588.
11 S. Cho, S.-H. Kim and D. Shin, *Eur. J. Med. Chem.*, 2019, **164**, 517–545.
12 T. R. Fagundes, B. Bortoleti, P. Camargo, V. Concato, F. Tomiotto-Pellissier, A. Carloto, C. Panis, M. Bispo, F. M. Junior and I. Conchon-Costa, *Anti-Cancer Agents Med. Chem.*, 2022, **22**, 1592–1600.
13 S. Suzen and E. Buyukbingol, *Farmaco Sci.*, 2000, **55**, 246–248.
14 M. M. Elbadawi, A. I. Khodair, M. K. Awad, S. E. Kassab, M. T. Elsaady and K. R. Abdellatif, *Molecules*, 2022, **1249**, 131574.
15 A. R. E. Mahdy, M. Y. Alfaifi, M. S. El-Gareb, N. Farouk and R. F. M. Elshaarawy, *Inorg. Chim. Acta*, 2021, **526**, 120504.
16 A. Kania, W. Tejchman, A. M. Pawlak, K. Mokrzyński, B. Różanowski, B. M. Musielak and M. Greczek-Stachura, *Molecules*, 2022, **27**, 1069.
17 J. Thanusu, V. Kanagarajan and M. Gopalakrishnan, *Bioorg. Med. Chem. Lett.*, 2010, **20**, 713–717.
18 T. H. Lee, Z. Khan, S. Y. Kim and K. R. Lee, *J. Nat. Prod.*, 2019, **82**, 3020–3024.
19 P. G. Camargo, B. T. d. S. Bortoleti, M. Fabris, M. D. Gonçalves, F. Tomiotto-Pellissier, I. N. Costa,

I. Conchon-Costa, C. H. d. S. Lima, W. R. Pavanelli and M. d.-L. F. Bispo, *J. Biomol. Struct. Dyn.*, 2022, **40**, 3213–3222.
20 B. T. da Silva Bortoleti, M. D. Gonçalves, F. Tomiotto-Pellissier, P. G. Camargo, J. P. Assolini, V. M. Concato, M. B. Detoni, D. L. Bidóia, M. d.-L. F. Bispo and C. H. da Silva Lima, *Chem. Biol. Interface*, 2022, **351**, 109690.
21 V. Singh, A. Singh, G. Singh, R. K. Verma and R. Mall, *Med. Chem. Res.*, 2021, **30**, 1905–1914.
22 P. G. Camargo, M. Fabris, T. U. da Silva, C. H. Silva Lima, S. de Paula Machado, L. T. D. Tonin, M. de Lima Ferreira Bispo and F. Macedo Jr, *ChemistrySelect*, 2021, **6**, 10429–10435.
23 C. H. Kwon, M. T. Iqbal and J. N. Wurpel, *J. Med. Chem.*, 1991, **34**, 1845–1849.
24 D. Mahajan, K. Chikhalia, C. Pannecouque and E. De Clercq, *Pharm. Chem. J.*, 2012, **46**, 165–170.
25 A. R. E. Mahdy, O. A. Abu Ali, W. M. Serag, E. Fayad, R. F. M. Elshaarawy and E. M. Gad, *J. Mol. Struct.*, 2022, **1259**, 132726.
26 A. A. Mourad, N. Farouk, E.-S. H. El-Sayed and A. R. Mahdy, *Life Sci.*, 2021, **277**, 119531.
27 I. Zaki, H. M. M. Ramadan, E.-S. H. El-Sayed and M. Abd El-Moneim, *J. Mol. Struct.*, 2020, **353**, 2000121.
28 S. N. Riduan and Y. Zhang, *Chem. Soc. Rev.*, 2013, **42**, 9055–9070.
29 F. Pandolfi, M. Bortolami, M. Feroci, A. Fornari, V. Scarano and D. Rocco, *Materials*, 2022, **15**, 866.
30 K. S. Egorova, E. G. Gordeev and V. P. Ananikov, *Chem. Rev.*, 2017, **117**, 7132–7189.
31 H. Hajfarajollaha, B. Mokhtarani, K. A. Noghabi, A. Sharifia and M. Mirzaei, *RSC Adv.*, 2014, **4**, 42751–42757.
32 R. F. M. Elshaarawy, I. M. Eldeen and E. M. Hassan, *J. Mol. Struct.*, 2017, **1128**, 162–173.
33 R. F. M. Elshaarawy, Y. Lan and C. Janiak, *Inorg. Chim. Acta*, 2013, **401**, 85–94.
34 Y. A. Hassan, A. I. M. Khedr, J. Alkabli, R. F. M. Elshaarawy and A. M. Nasr, *Carbohydr. Polym.*, 2021, **260**, 117834.
35 R. F. Elshaarawy, H. R. Tadros, R. M. Abd El-Aal, F. H. Mustafa, Y. A. Soliman and M. A. Hamed, *J. Environ. Chem. Eng.*, 2016, **4**, 2754–2764.
36 M. Ramadan, H. M. A. Hassan, A. Shahat, R. F. M. Elshaarawy and N. K. Allam, *New J. Chem.*, 2018, **42**(5), 3560–3567.
37 H. K. Ibrahim, S. H. El-Tamany, R. F. El-Shaarawy and I. M. El-Deen, *Maced. J. Chem. Chem. Eng.*, 2008, **27**, 65–79.
38 R. F. M. Elshaarawy, Z. H. Kheiralla, A. A. Rushdy and C. Janiak, *Inorg. Chim. Acta*, 2014, **421**, 110–122.
39 R. F. Elshaarawy, H. Abd El-Azim, W. H. Hegazy, F. H. Mustafa and T. A. Talkhan, *Polym. Test.*, 2020, **83**, 106244.
40 N. S. Alahmadi and R. F. J. Elshaarawy, *J. Mol. Liq.*, 2019, **281**, 451–460.
41 H.-A. Chu, H. Sackett and G. T. Babcock, *Biochem*, 2000, **39**, 14371–14376.
42 M. K. Trivedi, R. M. Tallapragada, A. Branton, D. Trivedi, G. Nayak, O. Latiyal and S. Jana, *Am. j. phys. appl.*, 2015, **3**, 215–220.
43 R. F. Elshaarawy and C. J. Janiak, *Tetrahedron*, 2014, **70**, 8023–8032.
44 H. M. A. Hassan, M. A. Betiha, E. A. El-Sharkawy, R. F. M. Elshaarawy, N. B. El-Assy, A. A. Essawy, A. M. Tolba and A. M. Rabie, *Colloids Surf., A*, 2020, **591**, 124520.
45 B. P. Gaber, V. Miskowski and T. G. Spiro, *J. Am. Chem. Soc.*, 1974, **96**, 6868–6873.
46 B. V. Trzhtsinskaya and N. D. Abramova, *Sulfur Rep.*, 1991, **10**, 389–421.
47 E. G. Jayasree and S. Sreedevi, *Chem. Phys.*, 2020, **530**, 110650.
48 K. Kobyłka, G. Żuchowski, W. Tejchman and K. K. Zborowski, *J. Mol. Model.*, 2019, **25**, 1–10.
49 H. Galbraith and T. Miller, *J. Appl. Bacteriol.*, 1973, **36**, 647–658.
50 A. Clements, F. Gaboriaud, J. F. Duval, J. L. Farn, A. W. Jenney, T. Lithgow, O. L. Wijburg, E. L. Hartland and R. A. Strugnell, *PLoS One*, 2008, **3**, e3817.
51 P. Mester, M. Wagner and P. Rossmanith, *Ecotoxicol. Environ. Saf.*, 2015, **111**, 96–101.
52 A. R. Dias, J. Costa-Rodrigues, M. H. Fernandes, R. Ferraz and C. Prudêncio, *ChemMedChem*, 2017, **12**, 11–18.
53 M. Y. Alfaifi, S. E. I. Elbehairi, R. F. Elshaarawy and M. A.-E. Zein, *J. Mol. Struct.*, 2022, **1249**, 131594.
54 S. Stolte, J. Arning, U. Bottin-Weber, M. Matzke, F. Stock, K. Thiele, M. Uerdingen, U. Welz-Biermann, B. Jastorff and J. Ranke, *Green Chem.*, 2006, **8**, 621–629.
55 L. He, D. Li, C. Zhang, P. Bai and L. Chen, *Bioorg. Med. Chem. Lett.*, 2017, **27**, 4171–4175.
56 B. Halliwell, *Drugs Aging*, 2001, **18**, 685–716.
57 A. Levina, A. Mitra and P. A. Lay, *Metallomics*, 2009, **1**, 458–470.